Thermal-property optimization dominated by the stoichiometric ratio in W-Si superconducting single-photon detectors

Zhi Qin,[1] Han Bao,[1] Tao Xu,[1] Shi Chen,[1] Shuchao Yang,[1] Haojie Li,[1] Zhihe Wang,[2] Xuecou Tu,[1,3] Labao Zhang,[1,4,5] Qingyuan Zhao,[1,3] Xiaoqing Jia[1,4,5,*] Guanghao Zhu,[1,4,†] Lin Kang,[1,4,5] Jian Chen,[1,3] and Peiheng Wu[1,4,5]

[1]*Institute of Superconducting Electronics (RISE), School of Electronic Science and Engineering, Nanjing University, Nanjing 210023, China*
[2]*School of Physics, Nanjing University, Nanjing 210023, China*
[3]*Purple Mountain Laboratory, Nanjing 211111, China*
[4]*Hefei National Laboratory, Hefei 230088, China*
[5]*Synergetic Innovation Center of Quantum Information and Quantum Physics, University of Science and Technology of China, Hefei, Anhui 230026, China*

Mid-infrared superconducting-nanowire single-photon detectors require higher detector sensitivity because of the weaker photon energy. Previous experiments demonstrated that the sensitivity of superconducting-nanowire single-photon detectors (SNSPDs) could be improved by optimizing the stoichiometry of superconducting films. However, the physical mechanism has not been completely studied. In this work, we attempt to explain the optimization mechanism from the hotspot dynamics point of view of thin films and detectors. We obtained the film's electron-transport parameters using magnetoconductance and Hall coefficient measurements and characterized the dynamic process of the hotspot based on the hotspot-relaxation time. Based on our experimental results, it is proposed that the stoichiometry of the W-Si film plays a role in the specific heat and boundary thermal conductivity, and therefore, affects the thermal relaxation process and the detector's sensitivity. The research results may lay the foundation for the development of highly efficient mid-infrared SNSPD.

I. INTRODUCTION

In recent years, superconducting-nanowire single-photon detectors (SNSPDs) have achieved high detection efficiency ($\sim$100%) [1], high count rates ($\sim$300 MHz) [2,3], low dark count rates ($\sim10^{-3}$ counts/s) [4], and low timing jitters (<3 ps) [5], making them the ideal single-photon detectors with comprehensive performance in the near-infrared band. Expanding such performance to the mid-infrared has potential applications in astronomical observation [6], dark-matter detection [7], and chemical spectral analysis [8].

Compared with near-infrared photons, the photon energy in the mid-infrared band is lower. Consequently, the quantum efficiency (QE) of the SNSPD greatly decreases in the mid-infrared band, limiting its application in this band. Therefore, improving the energy sensitivity in the mid-infrared band has become a crucial topic in the process of the development of mid-infrared single-photon detectors.

Previous approaches to improve the energy sensitivity of SNSPDs is to reduce the cross-section area of the nanowire by making the film thinner or the nanowire narrower [9,10]. With this approach, a $Mo_{0.8}Si_{0.2}$ SNSPD with 30-nm-wide nanowire was demonstrated to exhibit a saturated internal detection efficiency at 5 μm [10]. However, narrowing the nanowires can significantly impact the switching current due to defects, edge roughness, and width shrinkage. Additionally, when nanowires are narrowed to a certain extent, the superconductivity induced by the proximity effect will be suppressed, leading to nonsuperconducting behaviors [11]. Another approach to improve the energy sensitivity involves reducing the superconducting energy gap of the material. This results in a higher probability of breaking Cooper pairs (producing quasiparticles) for a given input energy [12]. Unfortunately, lowering the superconducting energy gap also reduces the critical temperature (T_c), thus resulting in a lower operating temperature.

---

*xqjia@nju.edu.cn
†ghzhu@nju.edu.cn

Recent experiments demonstrated that the energy sensitivity of SNSPDs could be improved by regulating the stoichiometric ratio of superconducting films [13–16]. In 2020, Verma *et al.* demonstrated that increasing the Si content in W-Si films reduced the carrier density, thereby increasing the effective temperature of each quasiparticle. With this approach, the nanobridge exhibited a response capability up to a wavelength of 9.9 μm [14]. Moreover in 2022, Colangelo *et al.* increased the Si content to over 50% and successfully operated a SNSPD at 7.4 μm [16]. It was suggested by the authors that the optimization mechanism was linked to a reduction of the density of states, which subsequently lowered the energy threshold of the detectors [16].

It should be noted that regulating the stoichiometry of the superconducting thin film not only modifies the density of states but also modifies the electron-transport properties and phonon-related properties (i.e., specific heat, thermal conductivity, etc.) of the film, and the last two will affect the dynamic process of the hotspots after optical excitation. Since the diffusion dynamics of hotspots plays a central role in the detection mechanism [17], regulating the stoichiometry of the films will thus affect the sensitivity of detectors through the impact of hotspots.

Here, we present a study of the influence of the stoichiometric regulation of W-Si thin films on the thermal relaxation and sensitivity issues of SNSPDs. We fabricated a series of W-Si films with different stoichiometric ratios by using the magnetron cosputtering system. From magnetoconductance and Hall coefficient measurements, we characterized the disorder of W-Si films with different stoichiometric ratios and obtained the film's electron-transport parameters. We also examined the impact of the thermal parameters of the W-Si film on the dynamic process of the hotspot by measuring the hotspot-relaxation time. The obtained experimental results suggest that the improvement of the detector's sensitivity is highly linked to the variation of electron transportation and the thermal properties, which are altered by optimization of the stoichiometric ratio of the W-Si film.

II. EXPERIMENT

A. Fabrication of W-Si film and SNSPDs

The fabrication method for the W-Si thin film is similar to those applied in previous studies [18,19]. W-Si thin films were deposited on a Si substrate by high-vacuum (base pressure $<1 \times 10^{-5}$ Pa) magnetron cosputtering. The size of the W target and Si target is 2 inches, and the purity is 99.99%. Both the W target and Si target were operated in constant-power mode. (Notably, the former was applied with direct-current power, while the latter was applied with radio-frequency power.) Initially, we introduced 23.1 sccm of argon in the process room, keeping the sputtering pressure at 1.0 Pa. During the sputtering process, the substrate

holder rotated at a speed of 50 rounds/min to improve the uniformity of the film. After depositing the W-Si film, we sputtered a Si layer about 2 nm thick in situ as a protective layer to prevent oxidation.

We fixed the Si target power at 100 W and controlled the stoichiometric ratio of W-Si films by adjusting the power on the W target (P_W). Figure 1(a) depicts the zero-resistance superconducting transition temperature (T_{C0}) of W-Si films (with a thickness of 100 nm) versus P_W. The T_{C0} of the films is above 5 K when the P_W is within the range from 40 to 50 W. We fabricated $W_{0.83}Si_{0.17}$, $W_{0.78}Si_{0.22}$, and $W_{0.73}Si_{0.27}$ films about 4.5 nm thick to study the effect of the stoichiometric ratio on detection performance. The chemical composition of these films was determined by using an Auger electron spectrometer (AES), as illustrated in Figs. 1(b)–1(d). Subsequently, we measured the T_{C0} of these thin films. The T_{C0} of $W_{0.78}Si_{0.22}$ and $W_{0.83}Si_{0.17}$ thin films is around 3.9 K, while the T_{C0} of $W_{0.73}Si_{0.27}$ is about 3.2 K [see Fig. 2(b)].

Thereafter, we fabricated three SNSPDs with identical nanowire patterns based on films made of $W_{0.83}Si_{0.17}$, $W_{0.78}Si_{0.22}$, and $W_{0.73}Si_{0.27}$. Ti/Au pads, which were lithographed using a lift-off process, and electron-beam lithography with PMMA950-A4 (Polymethyl methacrylate) was used to fabricate nanowires, which were sequentially etched in a gas mixture of CF_4 and Ar by reactive-ion etching. The active area of the detector was designed to be 15×15 μm^2 with a 100-nm meander size. As shown in Fig. 2(a), the width of the actual nanowires is consistent with the design value and shows uniformity.

B. Characterization of SNSPDs

The three SNSPDs were front coupled through a single-mode fiber and characterized at 1.6 K using a pulse tube cryocooler. The detectors were biased through a bias tee (ZFBT-6GW+ microcircuit) by a dc voltage source (Keithley 2400) with a 100-kΩ series resistor. The photon-generated pulse was amplified using a room-temperature amplifier (LNA-650) and sent to the counter (SR400).

The *I-V* curves of the three SNSPDs were measured, and the results are illustrated in Fig. 2(c). Our findings show that detectors with richer Si contents exhibit lower switch currents (I_{sw}). Note that the inset figure shows the difference of the hysteresis current (I_h), which is often associated with self-heating and thermal diffusion. The detectors were characterized by a 1550-nm pulse laser. Figure 2(d) displays the QE as a function of bias current for nine sets of detectors, with three detectors selected for each stoichiometric ratio. In Fig. 2(e), the bias currents of three representative detectors in Fig. 2(d) were normalized to their measured switch currents. We define the threshold bias current (I_{th}) by the bias point at which $\eta_{QE} = 0.95$, and the saturation region of the detector by the area above this threshold. With these definitions, it is
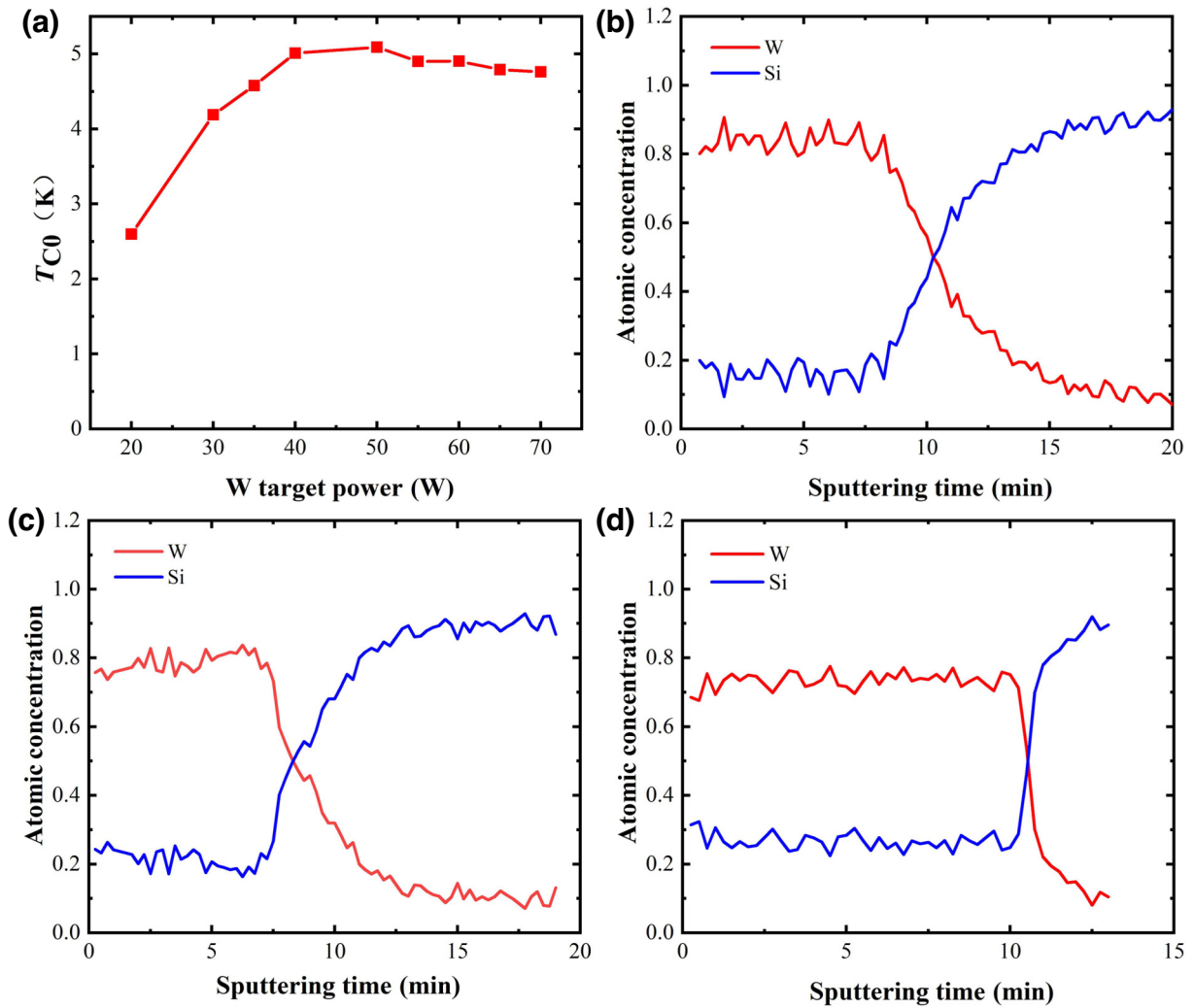
FIG. 1. (a) Superconducting transition temperature (T_{C0}) versus sputtering power of W target during cosputtering of W-Si film. AES results for the W-Si film, with (b) $W_{0.83}Si_{0.17}$, (c) $W_{0.78}Si_{0.22}$, and (d) $W_{0.73}Si_{0.27}$.

found that a detector with a richer Si content reaches the saturation region at a lower bias current. To investigate the wavelength dependence, we selected two representative detectors, $W_{0.78}Si_{0.22}$ and $W_{0.83}Si_{0.17}$, and measured their QEs at longer wavelengths using a continuous-wave laser that was tunable from 1600 to 1900 nm. The obtained results are presented in Fig. 2(f). For the same wavelength, the detector with richer Si contents exhibited a smaller normalized threshold current of I_{th}/I_{sw} and a higher ratio of the saturation region. These results indicate that, by regulating the stoichiometric ratio of the thin film, the detector's energy sensitivity can be improved and the cutoff wavelength can be effectively extended to longer wavelengths. On the other hand, it should also be noted that, as the Si content increases, the switching currents of the detectors decrease, resulting in a significant decrease in the signal-to-noise ratio and an increase in the jitter of the detector [20].

C. Characterization of W-Si films in a magnetic field

To investigate the underlying reason for the sensitivity improvement of the detector with richer Si content, crucial parameters of W-Si films with varying stoichiometric ratios were measured. We first measured the electrical transport characteristics of the films subject to a magnetic field. Figure 3(a) illustrates the temperature dependence of sheet resistance at different magnetic field intensities (ranging from 0 to 1.5 T). From Fig. 3(a), we extracted the upper critical magnetic field and plotted the results as a function of temperature in Fig. 3(b). Note that, in our work, the upper critical magnetic field, B_{C2}, is defined as the magnetic field at which $R = 0.5\ R_n$, where R_n is the resistance measured in the normal state. We obtained the upper critical magnetic field, B_{C2}, by fitting the data with the equation reported previously in Ref. [18]. Subsequently, we extracted the slope to further calculate the electron-diffusion coefficient, D, using the formula given in
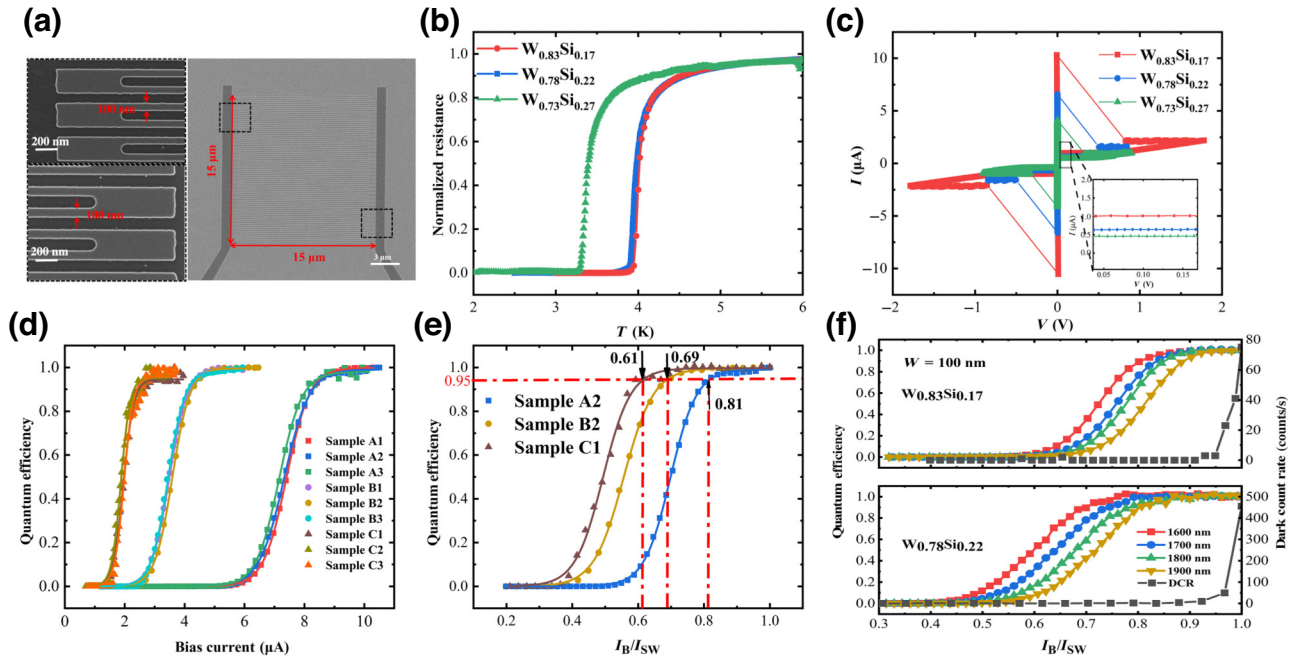
FIG. 2. (a) SEM image of the SNSPD detector. (b) *R-T* curves of the three types of films. (c) *I-V* curves of the three types of detectors. Inset figure is an enlargement of the I_h part. (d) QE at 1550 nm versus bias current of the nine sets of detectors at 1.6 K for samples A1–A3, $W_{0.83}Si_{0.17}$; samples B1–B3, $W_{0.78}Si_{0.22}$; and samples C1–C3, $W_{0.73}Si_{0.27}$. (e) QE at 1550 nm versus normalized bias current of the three detectors at 1.6 K. (f) QE in the wavelength range of 1600 to 1900 nm and dark count rate versus normalized bias current of the $W_{0.83}Si_{0.17}$ and $W_{0.78}Si_{0.22}$ detectors at 1.6 K.

Ref. [18]. Based on the diffusion coefficient, the electronic density of states at the Fermi level, N_0, is determined by

$$N_0 = 1/(De^2 R_{SN}d), \qquad (1)$$

where e is the electron charge, d is the film thickness, and R_{SN} is the sheet resistance of the film in the normal state [21]. The measured parameters are summarized in Table I, where it can be seen that the values of D and N_0

decrease with increasing Si contents in W-Si films. Note that when the value of D decreases, thermal diffusion along the nanowires is hindered during the hotspot-formation process [22]. Additionally, a smaller value of N_0 also implies a smaller value of electron heat capacity [23], which will lead to a higher hotspot temperature. Based on these findings, we believe it is reasonable to suggest that the improvement of the detection efficiency of the SNSPDs is caused by the modification of the hotspot-relaxation
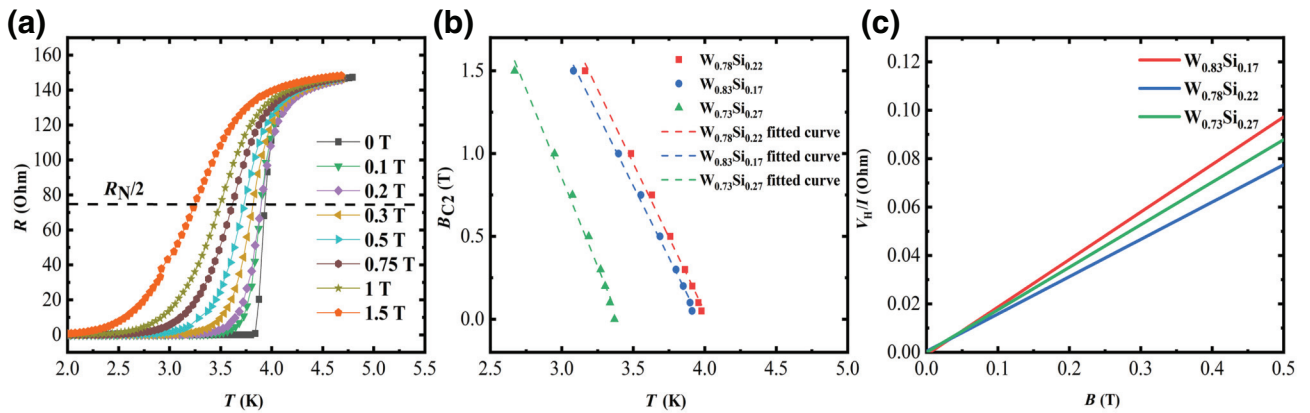

FIG. 3. (a) *R-T* curves of 4.5-nm W-Si thin films under different magnetic fields. (b) Upper critical magnetic field, B_{C2}, versus temperature of 4.5-nm $W_{0.78}Si_{0.22}$ (red), $W_{0.83}Si_{0.17}$ (blue), and $W_{0.73}Si_{0.27}$ (green). (c) Hall voltage divided by transmission current of 4.5-nm $W_{0.83}Si_{0.17}$ (red), $W_{0.78}Si_{0.22}$ (blue), and $W_{0.73}Si_{0.27}$ (green) versus magnetic field.

TABLE I.   Transport and superconducting parameters of three types of W-Si films reported in this work.

Sample	d (nm)	T_{C0} (K)	R_S (Ω)	D (cm^2/s)	N_0 (J^{-1} m^{-3})	$k_F l_e$
W$_{0.83}$Si$_{0.17}$	4.5	3.9	300	0.623	4.64×10^{47}	1.16
W$_{0.78}$Si$_{0.22}$	4.5	3.9	360	0.601	4.01×10^{47}	0.92
W$_{0.73}$Si$_{0.27}$	4.5	3.2	452	0.54	3.56×10^{47}	0.76

process, which results from the optimization of the stoichiometric ratio of W-Si films.

To provide further evidence that the hotspot-relaxation process is altered by the stoichiometric ratio, the Ioffe Regel parameters were measured for SNSPDs with different Si contents. Note that the Ioffe Regel parameter serves as a measure of the material disorder, which plays an important role in the hotspot-relaxation process of the superconducting films [24,25]. The Ioffe Regel parameter is the product of k_F (the Fermi wave vector) and l_e (the average free path of elastic electrons) and can be obtained by Hall coefficient measurements [21,26]. Here, we used the four-probe ac technology to carry out the Hall coefficient measurements at room temperature. A 1×1-mm^2 Hall bar on a 10×10-mm^2 sample was used to ensure the Ohmic contact. As shown in Fig. 3(c), the Hall voltage (V_H) varied linearly with the magnetic field if the magnetic field was in the range of ± 1 T. From these measurements, we obtained the Hall coefficient (R_H) by calculating the slope according to $R_H = V_H d/(IB)$, where I is the current and B is the magnetic field intensity applied to the sample. Using the Hall coefficient, R_H, the carrier density, n_e, can be obtained according to $n_e = -1/eR_H$. Finally, the Fermi wave vector (k_F), the average free path of elastic

electrons (l_e), and hence the Ioffe Regel parameter ($k_F l_e$) were determined [21]:

$$k_F = (3\pi^2 n_e)^{1/3}, \qquad (2)$$

$$l_e = \hbar k_F/(n_e e^2 R_{SN} d), \qquad (3)$$

where $\hbar$ is the reduced Planck constant. Through the measurement results, we found that the films with richer Si contents exhibited stronger disorder and were expected to suffer from hindered thermal relaxation and enlarged hotspot size [24].

III. DISCUSSION

The photoexcitation of hotspot regions is the foundation of SNSPD operation, and the relationship between hotspot dynamics and SNSPD sensitivity is discussed in detail in Ref. [27]. In this section, we focus on the hotspot-relaxation time [24,28–30] and investigate the hotspot dynamics of the SNSPDs with different Si contents. Note that the sensitivity of the detector is highly related to the cross-section area of the nanowire and the superconducting energy gap. For the W$_{0.78}$Si$_{0.22}$ and W$_{0.83}$Si$_{0.17}$ detectors, the closely related T_C allows us to investigate purely the influence of stoichiometry on detector sensitivity under the condition that the superconducting energy gaps are similar. Therefore, we mainly discuss the W$_{0.78}$Si$_{0.22}$ and W$_{0.83}$Si$_{0.17}$ detectors here. The hotspot-relaxation time, τ_{HS}, describes the energy-transfer and down-conversion process after photon absorption [28]. In previous experiments, we measured the hotspot-relaxation time of Nb-N nanowires with and without buffer layers using a two-photon detection mode [29]. Under low bias currents, a single photon's energy deposited on the nanowires is insufficient to generate a pulse, and the pulse can be triggered only if two photons generate two overlapping hotspots. Such a process is generally termed the two-photon detection mode [28], which provides a method for studying the formation and dissipation of the hotspot with subpicosecond resolution. It should be noted that, in the two-photon detection mode, the response of the detector is strongly related to the bias current. To make a fair comparison, we selected W$_{0.78}$Si$_{0.22}$ and W$_{0.83}$Si$_{0.17}$ detectors using the same normalized bias current of $I_B = 0.4\ I_{sw}$ and measured their delayed two-photon responses using the setup described in Ref. [29]. The measured results are presented
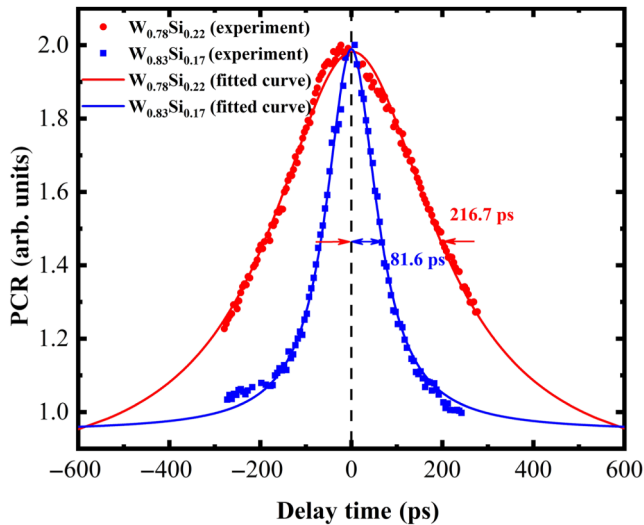

FIG. 4.   Average photon count per pulse (PCR) versus delay time in the two-photon operation mode, with W$_{0.78}$Si$_{0.22}$ (red) and W$_{0.83}$Si$_{0.17}$ (blue) detectors. Symbol, experimental data; line, Lorentz fitting.
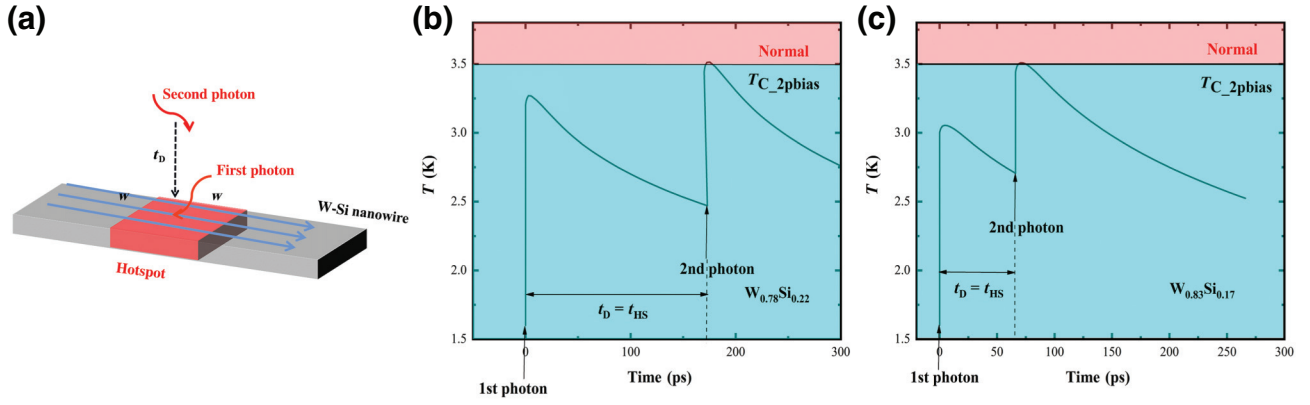
(a)

(b)

(c)

FIG. 5.   (a) Illustration of the two-photon detection mode. Simulated time evolution of T_{hot} after absorption of two subsequent photons for two detectors: (b) $W_{0.78}Si_{0.22}$, (c) $W_{0.83}Si_{0.17}$.

in Fig. 4, where it can be seen that, at $I_B = 0.4\ I_{sw}$, the relaxation time (216.7 ps) of the $W_{0.78}Si_{0.22}$ detector is approximately 2.6 times that of the $W_{0.83}Si_{0.17}$ detector (81.6 ps). These results reveal that a detector with a richer Si content takes a longer time to dissipate hotspots. Note that these values of the relaxation time of W-Si SNSPDs are significantly longer than those measured previously on the Nb-N SNSPDs (15–30 ps) [29].

To further investigate the mechanism that causes the difference in relaxation times for the different types of detectors, we developed a numerical model for two-photon relaxation experiments based on Ref. [28]. In our numerical two-photon model, it is assumed that a few picoseconds after absorption, the nonequilibrium distribution of the quasiparticle is generated through the electron-phonon and electron-electron interactions [31]. Since this process is expected to occur on a much shorter timescale than the experimental value of τ_{HS}, the initial evolution of the quasiparticle distribution can be ignored [28]. As shown in Fig. 5(a), we assume that the nanowire forms a square-shaped hotspot after the first photon is absorbed, where the temperature of the square hotspot (T_{hot1}) is higher than the bath temperature (T_{sub}). The subsequent relaxation of temperature in the hotspot area then follows [23]

$$-Cd\frac{\partial T}{\partial t} + j^2\rho d + dk\frac{\partial^2 T}{\partial x^2} - \sigma(T^4 - T_{sub}^4) = 0, \quad (4)$$

where the heat capacity, C, includes the electron specific heat, C_e, and the phonon specific heat, C_{ph} [23]. Due to the lowered bias current, the hotspot formed by one-photon absorption in the two-photon experiment cannot disrupt the superflow in the nanowire. Therefore, the Joule heating term ($j^2\rho d$), as triggered by the first photon, does not play a role and can be neglected. Heat transfer from the thin film to the substrate follows a fourth-power role [32], where σ describes the time for phonons to escape from the film [32] and may be significantly affected by defects and

acoustic mismatching between the film and substrate [30]. It thus follows that films with higher disorder are expected to have a smaller thermal boundary conductance. It should be noted that, according to Eq. (5), σ can be obtained from the hysteresis current [29]:

$$J_h = \left[\frac{\sigma}{4d\rho}(T_c^4 - T_{sub}^4) \right]^{0.5}. \quad (5)$$

Based on Eq. (5) and according to the *I-V* curves of the two detectors [see Fig. 2(b)], the values of σ for $W_{0.78}Si_{0.22}$ and $W_{0.83}Si_{0.17}$ are determined to be 291.6 and 636.8 W/m^2 K^4, respectively.

We simulated the temperature evolution of the two types of detectors under the two-photon region (with simulation parameters listed in Table II). The results are shown in Figs. 5(b) and 5(c). Following Ref. [28], after the first photon is absorbed, the temperature of the hotspot immediately increases from T_{sub} to T_{hot1}, and then gradually relaxes back toward T_{sub}. After a delay time of t_D, the second photon is absorbed, and the temperature of the hotspot rises to T_{hot2}. If the temperature (T_{hot2}) exceeds the critical temperature, T_c, at the applied bias current (T_{C2bias}), the hotspot switches to the normal state and clicks a response pulse. We define the theoretical hotspot-relaxation time as the maximum of t_D that meets $T_{hot2} > T_{C2bias}$. From Figs. 5(b) and 5(c), the theoretical hotspot-relaxation times of the two

TABLE II.   Parameters used in the thermal simulation of the $W_{0.78}Si_{0.22}$ and $W_{0.83}Si_{0.17}$ detectors reported in this work.

Parameters applied in simulation	$W_{0.78}Si_{0.22}$	$W_{0.83}Si_{0.17}$
C_e (@3.9 K) [J/(m^3 K)]	1957	2265
C_{ph} (@3.9 K) [J/(m^3 K)]	1397	1618
σ (W/m^2 K^4)	291.6	636.8
T_{C2bias} (K)	3.5	3.5
T_{sub} (K)	1.6	1.6

detectors are determined to be 175 and 65 ps, respectively; these values in a good agreement with the values measured above. Our numerical simulation thus supports the conclusion that detectors with a higher Si content would have a longer hotspot-relaxation time.

IV. CONCLUSION

Here, we investigated the effect of the stoichiometric ratios of W-Si films on the performance of SNSPDs. Through the characterization of W-Si films and detectors with different stoichiometric ratios, it is proposed that W-Si films with richer Si contents are more suitable for SNSPDs operating in the mid-infrared range because of their modified thermal properties, such as the specific heat and boundary thermal conductivity. This work may provide a feasible strategy for expanding the application wavelength of SNSPDs, including but not limited to W-Si, promoting the development of various applications of SNSPDs in the mid-infrared range.

ACKNOWLEDGMENTS

[1] J. Chang, J. Los, J. Tenorio-Pearl, N. Noordzij, R. Gourgues, A. Guardiani, J. Zichi, S. Pereira, H. Urbach, and V. Zwiller, Detecting telecom single photons with $99.5 - 2.07 + 0.5\%$ system detection efficiency and high time resolution, APL Photonics **6**, 036114 (2021).

[2] X. Tao, H. Hao, X. Li, S. Chen, L. Wang, X. Tu, X. Jia, L. Zhang, Q. Zhao, and L. Kang, Characterize the speed of a photon-number-resolving superconducting nanowire detector, IEEE Photonics J. **12**, 1 (2020).

[3] W. H. Pernice, C. Schuck, O. Minaeva, M. Li, G. Goltsman, A. Sergienko, and H. Tang, High-speed and high-efficiency travelling wave single-photon detectors embedded in nanophotonic circuits, Nat. Commun. **3**, 1325 (2012).

[4] H. Shibata, K. Shimizu, H. Takesue, and Y. Tokura, Ultimate low system dark-count rate for superconducting nanowire single-photon detector, Opt. Lett. **40**, 3428 (2015).

[5] B. Korzh, Q.-Y. Zhao, J. P. Allmaras, S. Frasca, T. M. Autry, E. A. Bersin, A. D. Beyer, R. M. Briggs, B. Bumble, and M. Colangelo, Demonstration of sub-3 ps temporal resolution with a superconducting nanowire single-photon detector, Nat. Photonics **14**, 250 (2020).

[6] M. Ressler, K. Sukhatme, B. Franklin, J. Mahoney, M. Thelen, P. Bouchet, J. Colbert, M. Cracraft, D. Dicken, and R. Gastaud, The mid-infrared instrument for the James Webb space telescope, VIII: The MIRI focal plane system, Publ. Astron. Soc. Pac. **127**, 675 (2015).

[7] Y. Hochberg, I. Charaev, S.-W. Nam, V. Verma, M. Colangelo, and K. K. Berggren, Detecting sub-GeV dark matter with superconducting nanowires, Phys. Rev. Lett. **123**, 151802 (2019).

[8] L. Chen, D. Schwarzer, V. B. Verma, M. J. Stevens, F. Marsili, R. P. Mirin, S. W. Nam, and A. M. Wodtke, Mid-infrared laser-induced fluorescence with nanosecond time resolution using a superconducting nanowire single-photon detector: New technology for molecular science, Acc. Chem. Res. **50**, 1400 (2017).

[9] F. Marsili, F. Bellei, F. Najafi, A. E. Dane, E. A. Dauler, R. J. Molnar, and K. K. Berggren, Efficient single photon detection from 500 nm to 5 μm wavelength, Nano Lett. **12**, 4799 (2012).

[10] Q. Chen, R. Ge, L. Zhang, F. Li, B. Zhang, F. Jin, H. Han, Y. Dai, G. He, and Y. Fei, Mid-infrared single photon detector with superconductor $Mo_{0.8}Si_{0.2}$ nanowire, Sci. Bull. **66**, 965 (2021).

[11] Q. Chen, B. Zhang, L.-b. Zhang, F.-y. Li, F.-f. Jin, H. Han, R. Ge, G.-l. He, H.-c. Li, and J.-r. Tan, Suppression of superconductivity dominated by proximity effect in amorphous MoSi nanobelts, Phys. Rev. B **105**, 014516 (2022).

[12] J. P. Allmaras, Ph.D. thesis, California Institute of Technology, 2020.

[13] Y. Pan, H. Zhou, L. Zhang, H. Li, Y. Tang, H. Yu, M. Si, L. You, and Z. Wang, Superconducting nanowire single-photon detector made of ultrathin γ-Nb_4N_3 film for mid-infrared wavelengths, Supercond. Sci. Technol. **34**, 074001 (2021).

[14] V. Verma, B. Korzh, A. B. Walter, A. E. Lita, R. M. Briggs, M. Colangelo, Y. Zhai, E. E. Wollman, A. D. Beyer, and J. P. Allmaras, Single-photon detection in the mid-infrared up to 10 μm wavelength using tungsten silicide superconducting nanowire detectors, APL Photonics **6**, 056101 (2021).

[15] J. Chiles, S. M. Buckley, A. Lita, V. B. Verma, J. Allmaras, B. Korzh, M. D. Shaw, J. M. Shainline, R. P. Mirin, and S. W. Nam, Superconducting microwire detectors based on WSi with single-photon sensitivity in the near-infrared, Appl. Phys. Lett. **116**, 242602 (2020).

[16] M. Colangelo, A. B. Walter, B. A. Korzh, E. Schmidt, B. Bumble, A. E. Lita, A. D. Beyer, J. P. Allmaras, R. M. Briggs, and A. G. Kozorezov, Large-area superconducting nanowire single-photon detectors for operation at wavelengths up to 7.4 μm, Nano Lett. **22**, 5667 (2022).

[17] A. D. Semenov, G. N. Gol'tsman, and A. A. Korneev, Quantum detection by current carrying superconducting film, Phys. C **351**, 349 (2001).

[18] H. Bao, T. Xu, C. Li, X. Jia, L. Kang, Z. Wang, Y. Wang, X. Tu, L. Zhang, and Q. Zhao, Characterization of

superconducting NbN, WSi and MoSi ultra-thin films in magnetic field, IEEE Trans. Appl. Supercond. **31**, 1 (2021).

[19] J. Jin, F. Fu, X. Jia, L. Kang, Z. Wang, X. Tu, L. Zhang, B. B. Jin, J. Chen, and W. Xu, Preparation and characterization of ultrathin WSi films for superconducting nanowire single-photon detectors, IEEE Trans. Appl. Supercond. **29**, 1 (2019).

[20] Lixing You, Xiaoyan Yang, Yuhao He, Wenxing Zhang, Dengkuan Liu, Weijun Zhang, Lu Zhang, Ling Zhang, Xiaoyu Liu, and Sijing Chen, Jitter analysis of a superconducting nanowire single photon detector, AIP Adv. **3**, 7 (2013).

[21] M. Sidorova, A. Semenov, H.-W. Hübers, S. Gyger, S. Steinhauer, X. Zhang, and A. Schilling, Magnetoconductance and photoresponse properties of disordered NbTiN films, Phys. Rev. B **104**, 184514 (2021).

[22] Konstantin Smirnov, Alexander Divochiy, Yury Vakhtomin, Pavel Morozov, Philipp Zolotov, Andrey Antipov, and Vitaliy Seleznev, NbN single-photon detectors with saturated dependence of quantum efficiency, Supercond. Sci. Technol. **31**, 035011 (2018).

[23] J. K. Yang, A. J. Kerman, E. A. Dauler, V. Anant, K. M. Rosfjord, and K. K. Berggren, Modeling the electrical and thermal response of superconducting nanowire single-photon detectors, IEEE Trans. Appl. Supercond. **17**, 581 (2007).

[24] L. Zhang, L. You, X. Yang, J. Wu, C. Lv, Q. Guo, W. Zhang, H. Li, W. Peng, and Z. Wang, Hotspot relaxation time of NbN superconducting nanowire single-photon detectors on various substrates, Sci. Rep. **8**, 1486 (2018).

[25] A. Leo, G. Grimaldi, R. Citro, A. Nigro, S. Pace, and R. Huebener, Quasiparticle scattering time in nio-

bium superconducting films, Phys. Rev. B **84**, 014536 (2011).

[26] S. Chockalingam, M. Chand, J. Jesudasan, V. Tripathi, and P. Raychaudhuri, Superconducting properties and Hall effect of epitaxial NbN thin films, Phys. Rev. B **77**, 214503 (2008).

[27] A. Kozorezov, C. Lambert, F. Marsili, M. Stevens, V. Verma, J. Stern, R. Horansky, S. Dyer, S. Duff, and D. Pappas, Quasiparticle recombination in hotspots in superconducting current-carrying nanowires, Phys. Rev. B **92**, 064504 (2015).

[28] F. Marsili, M. J. Stevens, A. Kozorezov, V. B. Verma, C. Lambert, J. A. Stern, R. D. Horansky, S. Dyer, S. Duff, and D. P. Pappas, Hotspot relaxation dynamics in a current-carrying superconductor, Phys. Rev. B **93**, 094518 (2016).

[29] T. Xu, S. Chen, H. Shi, X. Jia, L. Zhang, Q. Zhao, X. Tu, L. Kang, J. Chen, and P. Wu, Effect of buffer layer on thermal recovery of superconducting nanowire single-photon detector, Supercond. Sci. Technol. **34**, 074002 (2021).

[30] L. Zhang, L. You, X. Yang, Y. Tang, M. Si, K. Yan, W. Zhang, H. Li, H. Zhou, and W. Peng, Hotspot relaxation time in disordered niobium nitride films, Appl. Phys. Lett. **115**, 132602 (2019).

[31] D. Y. Vodolazov, Single-photon detection by a dirty current-carrying superconducting strip based on the kinetic-equation approach, Phys. Rev. Appl. **7**, 034014 (2017).

[32] A. Dane, J. Allmaras, D. Zhu, M. Onen, M. Colangelo, R. Baghdadi, J. L. Tambasco, Y. Morimoto, I. E. Forno, I. Charaev, Q. Zhao, M. Skvortsov, A. Kozorezov, and K. K. Berggren, Self-heating hotspots in superconducting nanowires cooled by phonon black-body radiation, Nat. Commun. **13**, 5429 (2022).